A DC-voltage Controlled Variable Capacitor for Stabilizing the ZVS Frequency of a Resonant Converter for Wireless Power Transfer

Jianlong Tian, *Student IEEE Member*, Aiguo Patrick Hu, *Senior IEEE Member*

***Abstract*—Varators are often used in PLL (phase locked loop) circuits for dynamic frequency control. However, the voltage and current ratings of varactors are too low to be used in most power electronic circuits. This paper proposes a transistor controlled variable capacitor (*TCVC*), which functions similar to varactors in that its equivalent capacitance can be controlled by a DC voltage. However, the *TCVC* can handle high voltages and currents so that it can be used in DC-AC power converters of Wireless Power Transfer (WPT) systems such as an autonomous push pull resonant converter to adjust its ZVS (zero voltage switching) frequency so that the operating frequency of the system can be stabilized to simplify the circuit and EMI filter design particularly for WPT systems with multiple power pickups, while maintaining soft-switching operation of the converter against magnetic coupling and load variations. The relationship between the equivalent capacitance of the *TCVC* and the DC control voltage is developed by theoretical analysis and verified by experimental results. A prototype circuit is built with a PLL controller to demonstrate that the soft-switching condition of the converter is maintained when the operating frequency is locked in at 1.65MHz under load and magnetic coupling variations.**

***Index Terms*—Frequency control, Inductive power transfer, Variable capacitor, Wireless power transfer.**

I. Introduction

DYNAMIC frequency adjustment is often needed for both low power radio systems and power electronic circuits. For example, it is of great importance to be able to adjust the operating frequency of wireless power transfer (WPT) systems dynamically so that soft-switching and resonant operation can be achieved for maximum power transfer and efficiency [1]-[5]. Traditionally, this is realized through switching mode capacitors [6]-[12] or inductors [13]-[20]. PWM signals instead of a DC voltage are used for their control, and the active switches in them may need gate drivers and a separate voltage source, which makes the circuit complex and sometimes inconvenient, for example when used at the secondary side of an IPT (inductive power transfer) system where an auxiliary power supply is not readily available. Furthermore, at high frequencies it is difficult for switch mode circuits to be accurately soft-switched due to practical detection delays, component accuracies, etc.

On the other hand, varactors are widely used for frequency control in radio engineering [21]-[24]. However, the voltage and current ratings of varactors are too low to be applied in power electronics circuits. This paper proposes a Transistor Controlled Variable Capacitor (TCVC) for dynamic frequency control of IPT systems. The equivalent capacitance of the TCVC can be controlled simply with a DC voltage similar to varactors so that the ZVS frequency of the system can be adjusted smoothly and therefore to reach very high (MHz) levels with low EMI (Electromagnetic Interference). As no active switching is involved in the TCVC, no switch mode gate drivers are needed, which makes the overall structure of the TCVC simpler. Besides, the TCVC can be used flexibly in different places of resonant circuits for parallel and series tuning, which is often required in wireless power transfer systems. With the availability of the TCVC, the mature PLL technology can be employed directly to lock the operating frequency of DC-AC converters such as the autonomous push pull converter which becomes a voltage controlled oscillator (VCO) when the TCVC is applied to its resonant tank. The basic operating principle of the TCVC is explained in section II. Section III presents the theoretical modelling of the TCVC by establishing the relationships of the equivalent capacitance of the TCVC and the ZVS frequency of the converter against the DC control voltage. Practical experimental results about the open-loop relationship between the ZVS frequency of the converter and the control voltage, and the closed-loop (with the PLL controller added) waveforms of the circuit are provided in section IV. Finally conclusion is drawn in section V.

II. The Proposed Method and Basic Operating Principle

To take advantage of the ZVS frequency changing with the variation of its resonant capacitor, an autonomous push pull converter as shown in Fig. 1 is used as an example to show how the *TCVC* works and explain its basic operating principle. It can be seen from Fig. 1 that the normal fixed value resonant capacitor of the autonomous push pull converter is replaced by the *TCVC* consisting of C_{up}, C_{dw}, D_c, Q_c and R_b as shown in the dashed box titled "*TCVC*". The equivalent capacitance of the *TCVC* can be controlled by the voltage V_c because V_c influences the conduction period of the diode D_c by controlling the base and collector currents i_b and i_c of the transistor Q_c. The higher V_c is, the larger i_b and i_c, and the larger i_c is, the higher the

Date of submission: 26 April 2016.
This work was supported in part by PowerbyProxi Ltd. New Zealand.
Jianlong Tian is with the Dept of Electrical and Computer Engineering, University of Auckland, New Zealand (e-mail: jtia983@aucklanduni.ac.nz).
Aiguo Patrick Hu is with the Dept of Electrical and Computer Engineering, University of Auckland, New Zealand (e-mail: a.hu@auckland.ac.nz).

voltage on the anode of the diode D_c and the longer D_c conducts. When the diode D_c conducts, the equivalent capacitance of the *TCVC* is the capacitance of C_{dw}. When the diode is off, the equivalent capacitance of the *TCVC* is approximately the capacitance of C_{up} and C_{dw} in series. As C_{dw} is bigger than C_{up} and C_{dw} in series, the longer the diode conducts, the larger the average equivalent capacitance of the *TCVC* is. By controlling the conduction period of the diode D_c, the voltage V_c controls the average equivalent capacitance of the *TCVC* and finally the ZVS frequency of the autonomous push pull converter.

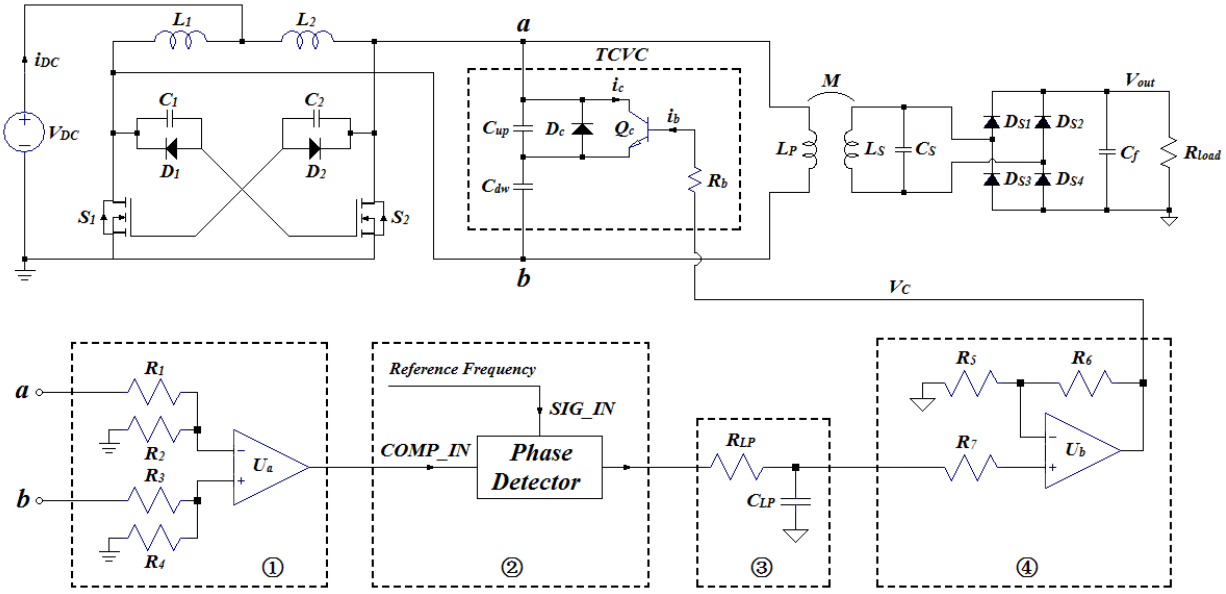

Fig. 1. The proposed *TCVC* in wireless power transfer system including autonomous push pull converter, pick-up circuit, and the PLL controller.

The parallel tuning full-bridge regulation pick-up circuit and the PLL controller are shown in Fig. 1 as well. The four dashed blocks ①, ②, ③ and ④ constitute the PLL controller, which generates the control voltage V_c automatically according to the difference between the ZVS frequency of the converter *COMP_IN* and a reference frequency *SIG_IN*. The ZVS frequency follows the reference frequency through the adjustment of the equivalent capacitance C_e. The function of the circuit block ① is to obtain the ZVS frequency of the converter through the resonant voltage v_{ab}. *Ua* is a differential comparator. v_{ab} are fed into *Ua* via the four resistors R_1~R_4 which function as voltage dividers. The output of *Ua-COMP_IN* is fed into the phase detector ② where *COMP_IN* is compared with the reference frequency *SIG_IN*. The output of the phase detector goes through the low pass filter ③ and becomes a DC voltage changing between 0~5V according to the difference between *COMP_IN* and *SIG_IN*. The function of the circuit block ④ is to amplify the 0~5V DC voltage from the low pass filter to generate the control voltage V_c. The whole control loop is implemented with analogue circuits without employing any digital sampling, microcontroller, etc. so that the operation is very fast and can run at very high frequencies.

III. THEORETICAL MODELLING

Based on the fact that the voltage of the resonant tank (v_{ab}) of the autonomous push pull converter is approximately a sine wave, the autonomous push pull converter shown in Fig.1 is simplified as the one shown in Fig.2 (a), which includes only the sinusoidal source v_s and the *TCVC*, where i_c represents the collector current of Q_c. Fig.2 (b) shows the situation when the *TCVC* is replaced by its equivalent capacitance C_e.

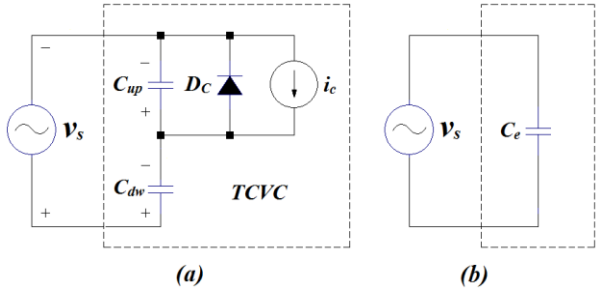

Fig. 2. The simplified circuit for theoretical analysis and derivation of approximate equivalent capacitance of the *TCVC*.

Fig. 3 shows the typical wave forms of the circuit in steady state including the voltage source-v_s, the voltage across the capacitor C_{up} and the diode D_c -v_{Cup}, the current flowing through the diode D_c - i_D and the current of the capacitor C_{up}-i_{Cup}. It can be seen from Fig. 3 that the voltage across the diode (v_{Cup}) is zero at both of the moments when the diode is turned on and off, which means that the diode is zero voltage switched. The current of the diode i_D reduces to zero gradually before the diode turns off, so the diode reverse recovering is less an issue. This helps the passive diode to operate at a fully soft switched condition, making the *TCVC* suitable for high frequency operation.

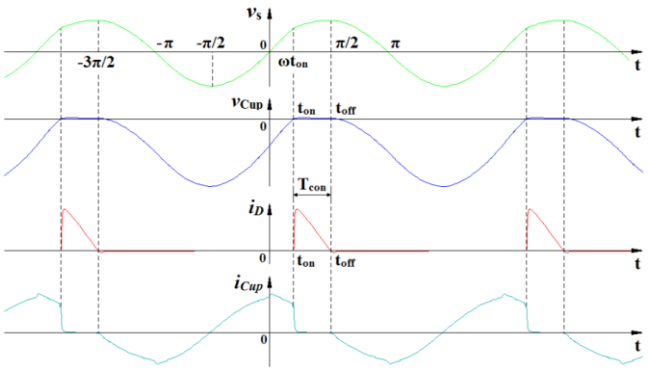

Fig. 3. Typical wave forms of the *TCVC*: v_S, v_{Cup}, i_D and i_{Cup}.

As the equivalent capacitance C_e of the *TCVC* plays a central role for the proposed method, the major task of the theoretical analysis is to find the relationship between C_e and the control voltage V_c, which is achieved in three steps. Firstly the relationship between the diode conduction period T_{con} and V_c is to be found. Secondly it is to find the relationship between C_e and T_{con}. Finally the relationship between C_e and V_c can be derived based on the above two relationships.

A. The relationship between T_{con} and V_c

Before the relationship between T_{con} and V_c is derived, two exact moments, i.e. the moment the diode starts to conduct "t_{on}" and the moment the diode stops to conduct 't_{off}" need to be determined first. Then T_{con} can be calculated with (1):

$$T_{\text{con}} = t_{\text{off}} - t_{\text{on}} \tag{1}$$

Fig. 4 shows the equivalent circuit of Fig. 2 (a) when the diode is conducting, got by removing C_{up}, D_c and i_c, as an ideal conducting diode amounts to a short-circuit. "i_s" in Fig. 4 represents the current flowing through the conducting diode D_c. D_c is regarded as stopping to conduct when i_s drops to zero.

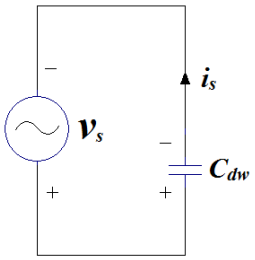

Fig. 4. The equivalent circuit when the diode is conducting.

As i_s drops to zero when the voltage V_s reaches its maximum at π/2, the moment the diode stops to conduct t_{off} can be express by (2).

$$t_{\text{off}} = \frac{\pi}{2\omega} \tag{2}$$

Fig. 5 shows the equivalent circuit of Fig. 2 (a) when the diode is not conducting, regarded as open and removed from the circuit. The diode is regarded as starting to conduct when the voltage V_{Cup} becomes zero.

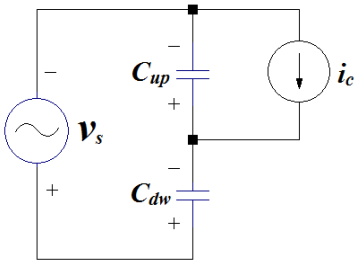

Fig. 5. The equivalent circuit when the diode is not conducting and the transistor is modelled as a current source.

Assume $v_s = A_s sin\omega t$, the equation governing V_{Cup} is :

$$\frac{dv_{Cup}}{dt} = \frac{\omega A_s C_{dw} cos\omega t + i_c}{C_{up}+C_{dw}} \tag{3}$$

The solution of (3) is:

$$v_{Cup} = \frac{A_s C_{dw}}{C_{up}+C_{dw}} sin\omega t + \frac{i_c}{C_{up}+C_{dw}} t + K \tag{4}$$

To determine the integral constant K in (4), substitute the initial condition (t= -3π/2ω and V_{Cup} =0 as shown in Fig. 3) into (4), gives:

$$K = \frac{\frac{3\pi}{2\omega} I_C - A_s C_{dw}}{C_{up}+C_{dw}} \tag{5}$$

Equation (4) expresses V_{Cup} during the period the diode is off. The moment the diode starts to conduct t_{on} is when V_{Cup} becomes zero as expressed by (6):

$$\frac{A_s C_{dw}}{C_{up}+C_{dw}} sin\omega t_{on} + \frac{i_c}{C_{up}+C_{dw}} t_{on} + K = 0 \tag{6}$$

There is no accurate analytical solution for (6). However, using Taylor's series and ignoring the high order terms gives: $sin\omega t_{on} = \omega t_{on}$. Substitute it into (6), an approximate analytical solution of t_{on} can be obtained as:

$$t_{on} \approx -\frac{K(C_{up}+C_{dw})}{\omega A_s C_{dw} + i_c} \tag{7}$$

Substitute (2) and (7) into (1) gives the relationship between T_{con} and i_c.

$$T_{con} \approx \frac{\pi}{2\omega} + \frac{K(C_{up}+C_{dw})}{\omega A_s C_{dw} + i_c} \tag{8}$$

Assuming the amplification of the transistor Q_c is β, the relationship between i_c and V_c can be expressed by (9):

$$I_C = \beta \cdot \frac{V_c - 0.7}{R_b} \tag{9}$$

Substituting (5) and (9) into (8) gives the relationship between T_{con} and V_c.

$$T_{con} \approx \frac{\pi}{2\omega} + \frac{\frac{3\pi}{2\omega}\beta - \frac{R_b A_s C_{dw}}{V_c - 0.7}}{\beta + \omega \frac{R_b A_s C_{dw}}{V_c - 0.7}} \tag{10}$$

Fig. 6 shows the theoretical relationship between T_{con} and V_c got from (10) using parameters of the components shown in Table 1 of section IV, from which it can be seen that a higher V_c leads to a longer diode conduction period as explained in section II. When V_c goes to infinite, (10) becomes " $T_{\rm con} \approx \frac{2\pi}{\omega}$ ", which means that $T_{\rm con}$ cannot go beyond the period of the oscillation of the circuit $\frac{2\pi}{\omega}$ in theory.

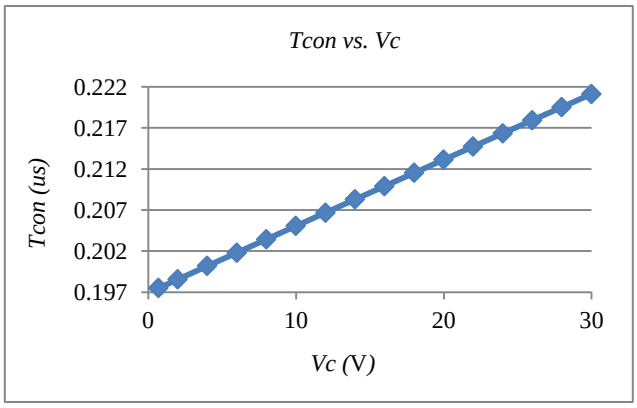

Fig. 6. Theoretical relationship between the diode conduction period T_{con} and the control voltage V_c.

B. *The relationship between C_e and T_{con}*

The relationship between C_e and T_{con} is derived based on the circuit shown in Fig. 2, and the idea that the AVECD (absolute value of the electric charge and discharge) of the *TCVC* equals that of its equivalent capacitance C_e during one cycle of the sinusoidal source $v_{\rm s}$. The AVECD of a capacitor C during the period from t_1 to t_2 when the voltage across the capacitor is "v" can be calculated by (11):

$$|\Delta Q| = \int_{t1}^{t2} |i(t)| \cdot dt = \int_{t1}^{t2} C \cdot |v'| \cdot dt \tag{11}$$

where $i(t)$ is the current flowing through the capacitor during the period. As the value of v' is positive when "v" increases and negative when "v" decreases, $|\Delta Q|$ is derived by calculating its values during the periods that "v" increases and decreases, respectively, and adding the results together by taking the negative value of " ΔQ " into consideration during the period when "v" decreases. (11) is used to calculate the various AVECD below. The reason to use the AVECD instead of the real value of electric charge and discharge is that the total real value of electric charge and discharge during one cycle of the sinusoidal source $v_{\rm s}$ is zero.

The equivalent capacitance C_e is calculated in three steps. Firstly, the AVECD of the *TCVC* - $|\Delta Q_{\rm TCVC}|$ is calculated. Secondly, the AVECD of the equivalent capacitance C_e-$|\Delta Q_{\rm Ce}|$ is calculated. Finally, C_e is derived by equating $|\Delta Q_{\rm TCVC}|$ and $|\Delta Q_{\rm Ce}|$.

$|\Delta Q_{\rm TCVC}|$ needs to be calculated in two periods-when the diode is on and off represented by $|\Delta Q_{\rm Don}|$ and $|\Delta Q_{\rm Doff}|$, respectively, while the calculation of $|\Delta Q_{\rm Doff}|$ is divided into two parts as well, i.e. the AVECD by the sinusoidal source $v_{\rm s}$ and the AVECD by the current source $i_{\rm c}$ represented by $|\Delta Q_{vs}|$ and $|\Delta Q_{ic}|$, respectively. As a result, $|\Delta Q_{\rm TCVC}|$ includes three parts-$|\Delta Q_{\rm Don}|$, $|\Delta Q_{vs}|$ and $|\Delta Q_{ic}|$ as calculated below:

$$\begin{aligned} |\Delta Q_{Don}| &= \int_{\omega t_{on}}^{\frac{\pi}{2}} C_{on}(A_s sin\omega t)' d(\omega t) \\ &= C_{on} A_s (1 - sin\omega t_{on}) \end{aligned} \tag{12}$$

As can be seen from Fig. 3, the "on" period of the diode is from ωt_{on} to $\frac{\pi}{2}$ when $v_{\rm s}$ increases.

$$\begin{aligned} |\Delta Q_{vs}| &= -\int_{-\frac{3\pi}{2}}^{-\frac{\pi}{2}} C_{off} \cdot (A_s sin\omega t)' d(\omega t) \\ &\quad + \int_{-\frac{\pi}{2}}^{\omega t_{on}} C_{off} \cdot (A_s sin\omega t)' d(\omega t) \\ &= C_{off} A_s (3 + sin\omega t_{on}) \end{aligned} \tag{13}$$

As can be seen from Fig. 3, the "off" period of the diode is from $-\frac{3\pi}{2}$ to ωt_{on}, which is divided into two periods "from $-\frac{3\pi}{2}$ to $-\frac{\pi}{2}$, and $-\frac{\pi}{2}$ to ωt_{on}", when $v_{\rm s}$ decreases and increases, respectively.

$$|\Delta Q_{ic}| = i_c \cdot \Delta t = i_c \frac{\omega t_{on} + \frac{3\pi}{2}}{\omega} \tag{14}$$

where Δt is the period during which the diode is off, i.e. from $-\frac{3\pi}{2}$ to ωt_{on}, which should be in the form of the absolute time instead of radians.

$|\Delta Q_{\rm TCVC}|$ is calculated by summing up (12), (13) and (14):

$$\begin{aligned} |\Delta Q_{TCVC}| &= |\Delta Q_{Don}| + |\Delta Q_{vs}| + |\Delta Q_{ic}| \\ &= A_s[3C_{\rm off} + C_{on} \\ &\quad + (C_{\rm off} - C_{on}) sin\omega t_{on}] \\ &\quad + i_c \left(t_{on} + \frac{3\pi}{2\omega}\right) \end{aligned} \tag{15}$$

The C_{on} and $C_{\rm off}$ in (12), (13), (14) and (15) means the instant capacitance of the *TCVC* during the period the diode is on and off, respectively as expressed by (16) and (17).

$$C_{on} = C_{dw} \tag{16}$$

$$C_{\rm off} = \frac{C_{up} C_{dw}}{C_{up} + C_{dw}} \tag{17}$$

The AVECD of the equivalent capacitance $C_{\rm e}$ during one cycle of the sinusoidal voltage source $v_{\rm s}$ can be calculated by (18):

$$|\Delta Q_{Ce}| = -\int_{-\frac{3\pi}{2}}^{-\frac{\pi}{2}} C_e(A_s sin\omega t)' d(\omega t) + \int_{-\frac{\pi}{2}}^{\frac{\pi}{2}} C_e(A_s sin\omega t)' d(\omega t) = 4C_e A_s \quad (18)$$

The calculation of $|\Delta Q_{Ce}|$ is divided into two periods "from $-\frac{3\pi}{2}$ to $-\frac{\pi}{2}$, and $-\frac{\pi}{2}$ to $\frac{\pi}{2}$," because it can be seen from Fig. 3 that v_s decrease and increase during these two periods, respectively so that v_s' is negative and positive accordingly which provides convenience for the calculation of the absolute value.

By equating (15) and (18), the equivalent capacitance C_e of the *TCVC* can finally be derived as:

$$C_e = \frac{3C_{off} + C_{on} + (C_{off} - C_{on})sin\omega t_{on}}{4} + \frac{t_{on} + \frac{3\pi}{2\omega}}{4A_s} \cdot i_c \quad (19)$$

As "t_{off}" is a fixed value $\frac{\pi}{2\omega}$, only "t_{on}" appears in (19).

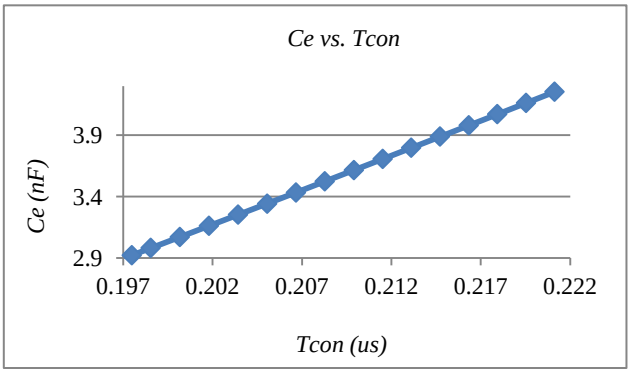

Fig. 7. Theoretical relationship between the equivalent capacitance C_e and the diode conduction period T_{con}.

By calculating T_{con} with (10) and C_e with (19), the relationship between C_e and T_{con} can be obtained as shown in Fig. 7 using parameters of the components shown in Table 1 of section IV, from which it can be seen that the longer the diode conducts, the larger the equivalent capacitance of the *TCVC* is as explained in section II.

C. The relationship between C_e and V_c

Substitute (9) into (19) gives the relationship between C_e and V_c:

$$C_e = \frac{3C_{off} + C_{on} + (C_{off} - C_{on})sin\omega t_{on}}{4} + \frac{\beta\left(t_{on} + \frac{3\pi}{2\omega}\right)}{4A_s R_b} \cdot (V_c - 0.7) \quad (20)$$

where: t_{on} is expressed by (7). As the relationships of T_{con} and V_c, and C_e and T_{con} as shown in Fig. 6 and Fig. 7 are proportionate, it can be deduced that C_e is proportional to V_c as well, which is in consistent with the theoretical and experimental results shown in Fig. 9 of section IV that the operating frequency f decreases with the control voltage V_c.

D. The relationship between f and V_c

Strictly speaking, what the voltage V_c controls is the ZVS frequency of the autonomous push pull converter. However, when the circuit quality factor Q is high, the ZVS frequency is close to the undamped natural oscillation frequency as expressed by (21) [24].

$$f = \frac{1}{2\pi\sqrt{LC}} \quad (21)$$

Substituting (20) into (21) gives the relationship between the approximate ZVS frequency of the converter and the control voltage V_c as expressed by (22):

$$f = \frac{1}{2\pi\sqrt{L\left[\frac{3C_{off} + C_{on} + (C_{off} - C_{on})sin\omega t_{on}}{4} + \frac{\beta\left(t_{on} + \frac{3\pi}{2\omega}\right)}{4A_s R_b} \cdot (V_c - 0.7)\right]}} \quad (22)$$

IV. Experimental Results

Fig. 8 shows the experimental setup (the same circuit as shown in Fig. 1).

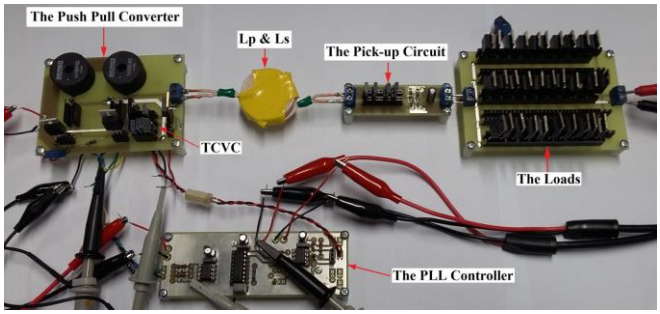

Fig. 8. The experimental setup.

As can be seen, it includes the push pull converter, the *TCVC*, the primary and secondary side coils L_P and L_S, the pick-up circuit and the PLL controller. Such a configuration may be suitable for low power contactless battery charging applications with very small physical separation between the primary and secondary coils.

Table 1 and 2 show the components and parameters of the primary and secondary side circuits, and the parameters of the coils, respectively.

Fig. 9 shows the open-loop (without the PLL controller) experimental and theoretical relationships between the operating frequency of the converter and the control voltage V_c together under two different situations when there is (R_{load}=100Ω) and there is no load, from which it can be seen

that the theoretical and experimental results agree with each quite well, and the operating frequency is negatively related to the control voltage V_c as explained in section II and III.

Table 1 Parameters and components of the primary and secondary side circuits.

V_{DC} (V)	L_1, L_2 (mH)	C_1, C_2 (nF)	D_1, D_2	S_1, S_2
12	1	5.5	BYV26C	IRF3205
C_{up} (nF)	C_{dw} (nF)	D_c	Q_c	R_b (kΩ)
1	50	C3D02060F	KSE13003	12
k	C_S (nF)	D_{S1}~D_{S4}	C_f (uF)	R_{load} (Ω)
0.62	4	PMEG10020AELRX	10	100

Table 2 Parameters of the primary and secondary side coils L_P and L_S.

No iron cores	Value (uH)	Number of turns	Diameter of the coil (mm)	Diameter of the litz wire (mm)	Distance between L_P and L_S (mm)
L_P	1.06	7	36.5	2.2	2.8
L_S	1.35	8	40	2.2	2.8

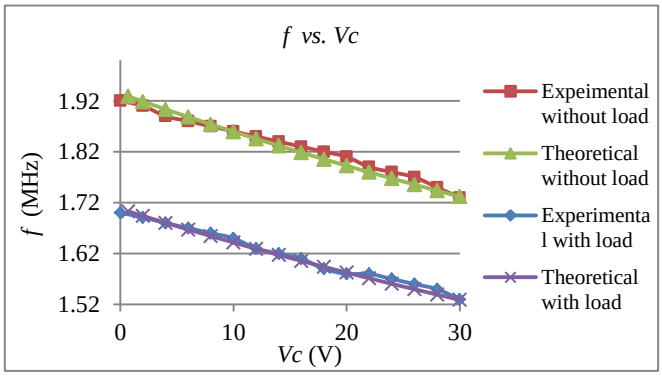

Fig. 9. Experimental and theoretical relationship between the operating frequency of the converter and the control voltage.

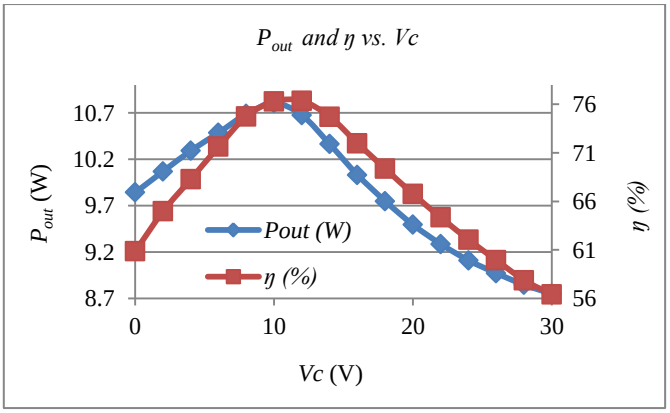

Fig. 10. Experimental relationships of the output power P_{out} (W) and efficiency η (%) vs. the control voltage V_c.

Fig. 10 shows the open-loop experimental relationships of the output power P_{out} and efficiency η (%) against the control voltage V_c, from which it can be seen that the output power and efficiency reach maximum of 10.8W and 74.7%, respectively with the control voltage V_c is around 10V, when the operating frequency of the converter is about 1.65MHz (refer to Fig. 9). The efficiency η (%) is calculated as the ratio of the output power (V_{out}^2/R_{load}) to the input power (V_{DC}*i_{DC}), where V_{DC} and i_{DC} are the voltage and current of the DC voltage source, respectively.

Fig. 11 shows the closed-loop waveforms (with the PLL controller added) of the voltage v_a at the point "a" of the resonant tank (channel 1), the signal *COMP_IN* after the comparator U_a (channel 2), the reference frequency *SIG_IN* (channel 3) and the output voltage of the PLL controller V_c (channel 4) when the reference frequency is set at 1.65MHz.

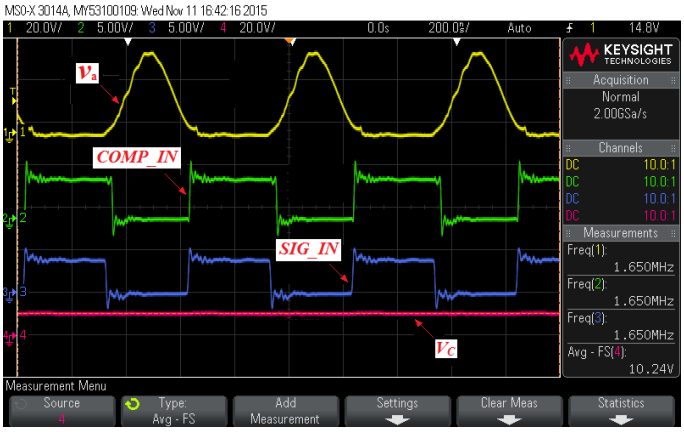

Fig. 11. Experimental waveforms of *va*, *COMP_IN*, *SIG_IN* and V_c when the reference frequency is set at 1.65MHz.

It can be seen from Fig. 11 that the frequencies of all the first three channels v_a, *COMP_IN* and *SIG_IN* are 1.65MHz, which means that the operating frequency of the converter is locked in at 1.65MHz by the PLL controller through adjusting the equivalent capacitance of the *TCVC* with the control voltage V_c, when the output power and voltage reach their maximum of 10.8 W and 32.87 V, respectively with the load resistance R_{load} is 100Ω and the coupling coefficient k is 0.62. In the experiment, the operating frequency can remain to be locked at 1.65MHz with the load resistance and the coupling coefficient k changing between 50Ω to 250Ω, and 0.62 to 0.53, respectively.

V. Conclusion

A transistor controlled variable capacitor (*TCVC*) was introduced in the paper for dynamic frequency control of resonant converters for wireless power transfer. The proposed method does not involve active switching and the ZVS frequency of the converter can be adjusted by a stable DC voltage so that the overall EMI can be reduced compared to traditional switch mode capacitors, and it can be potentially used for high frequency operation. A PLL controller is designed in combination with the *TCVC* for dynamic frequency control of the autonomous push pull converter. The operating frequency is locked in at the resonant value of 1.65MHz when the power transferred reaches its maximum of 10.8W in the experiment. The frequency can be maintained at 1.65MHz

under the load resistance and coupling coefficient *k* variations between 50Ω to 250Ω, and 0.62 to 0.53, respectively. The characteristics of the *TCVC* demonstrated from this fundamental research show that the proposed method can be widely used in many applications such as dynamic frequency control of resonant converters, circuit tuning/detuning for soft-switched operation, reactive power control, and the output voltage regulation of wireless power transfer systems.

REFERENCES

[1] N. Kim, K. Kim, J. Choi, and C.-W. Kim, "Adaptive frequency with power-level tracking system for efficient magnetic resonance wireless power transfer," *Electronics Letters*, vol. 48, pp. 452-454, 2012.

[2] N. Y. Kim, K. Y. Kim, and C. W. Kim, "Automated frequency tracking system for efficient mid-range magnetic resonance wireless power transfer," *Microwave and Optical Technology Letters*, vol. 54, pp. 1423-1426, 2012.

[3] H. Li, X. Yang, K. Wang, and X. Dong, "Study on efficiency maximization design principles for Wireless Power Transfer system using magnetic resonant coupling," in *ECCE Asia Downunder (ECCE Asia), 2013 IEEE*, 2013, pp. 888-892.

[4] J. Park, Y. Tak, Y. Kim, Y. Kim, and S. Nam, "Investigation of adaptive matching methods for near-field wireless power transfer," *Antennas and Propagation, IEEE Transactions on*, vol. 59, pp. 1769-1773, 2011.

[5] A. P. Sample, D. A. Meyer, and J. R. Smith, "Analysis, experimental results, and range adaptation of magnetically coupled resonators for wireless power transfer," *Industrial Electronics, IEEE Transactions on*, vol. 58, pp. 544-554, 2011.

[6] S. Ping, A. P. Hu, S. Malpas, and D. Budgett, "Switching Frequency Analysis of Dynamically Detuned ICPT Power Pick-ups," in *Power System Technology, 2006. PowerCon 2006. International Conference on*, 2006, pp. 1-8.

[7] A. W. Green and J. Boys, "10 kHz inductively coupled power transfer-concept and control," in *Power Electronics and Variable-Speed Drives, 1994. Fifth International Conference on*, 1994, pp. 694-699.

[8] P. Si, A. P. Hu, D. Budgett, S. Malpas, J. Yang, and J. Gao, "Stabilizing the operating frequency of a resonant converter for wireless power transfer to implantable biomedical sensors," in *Proc. 1st Int. Conf. Sensing Technology*, 2005, pp. 477-482.

[9] O. Abutbul, A. Gherlitz, Y. Berkovich, and A. Ioinovici, "Step-up switching-mode converter with high voltage gain using a switched-capacitor circuit," *Circuits and Systems I: Fundamental Theory and Applications, IEEE Transactions on*, vol. 50, pp. 1098-1102, 2003.

[10] G. A. Covic, J. T. Boys, A. M. W. Tam, and J. C. H. Peng, "Self tuning pick-ups for inductive power transfer," in *Power Electronics Specialists Conference, 2008. PESC 2008. IEEE*, 2008, pp. 3489-3494.

[11] P. Si, A. P. Hu, S. Malpas, and D. Budgett, "A frequency control method for regulating wireless power to implantable devices," *Biomedical Circuits and Systems, IEEE Transactions on*, vol. 2, pp. 22-29, 2008.

[12] F. Rodes, M. Zhang, R. Denieport, and X. Wang, "Optimization of the Power Transfer Through Human Body with an Auto Tuning System Using a Synchronous Switched Capacitor."

[13] D. C. Hamill and M. T. Bina, "The bootstrap variable inductance and its applications in AC power systems," in *Applied Power Electronics Conference and Exposition, 1999. APEC '99. Fourteenth Annual*, 1999, pp. 896-902 vol.2.

[14] T. Ishikawa, H. Funato, T. Ohtaki, and K. Kamiyama, "Transmission power control using variable inductance with feedforward-and feedback-based power controllers," in *Power Electronics and Drive Systems, 1999. PEDS'99. Proceedings of the IEEE 1999 International Conference on*, 1999, pp. 46-51.

[15] J. James, J. Boys, and G. Covic, "A variable inductor based tuning method for ICPT pickups," in *Power Engineering Conference, 2005. IPEC 2005. The 7th International*, 2005, pp. 1142-1146 Vol. 2.

[16] P. Park, C. S. Kim, M. Y. Park, S. Do Kim, and H. K. Yu, "Variable inductance multilayer inductor with MOSFET switch control," *Electron Device Letters, IEEE*, vol. 25, pp. 144-146, 2004.

[17] A. Tanabe, K. Hijioka, H. Nagase, and Y. Hayashi, "A Novel Variable Inductor Using a Bridge Circuit and Its Application to a 5–20 GHz Tunable LC-VCO," *Solid-State Circuits, IEEE Journal of*, vol. 46, pp. 883-893, 2011.

[18] L. Yo-Sheng, L. Hsiao-Bin, C. Jia-Lun, C. Ke-Hou, and L. Shey-Shi, "Variable Inductance Planar Spiral Inductors and CMOS Wideband Amplifiers with Inductive Peaking," in *Electron Devices and Solid-State Circuits, 2005 IEEE Conference on*, 2005, pp. 63-66.

[19] M. LIU, H. ZHANG, G. CHEN, and W. GONG, "Analysis and Design of A New Numerical Control Variable Inductance," *Chinese Journal of Electron Devices*, vol. 4, p. 007, 2012.

[20] J.-U. Hsu and A. P. Hu, "Determining the variable inductance range for an LCL wireless power pick-up," in *Electron Devices and Solid-State Circuits, 2007. EDSSC 2007. IEEE Conference on*, 2007, pp. 489-492.

[21] C. Huang, K. Buisman, M. Marchetti, L. K. Nanver, F. Sarubbi, M. Popadic, T. L. Scholtes, H. Schellevis, L. E. Larson, and L. C. de Vreede, "Ultra linear low-loss varactor diode configurations for adaptive RF systems," *Microwave Theory and Techniques, IEEE Transactions on*, vol. 57, pp. 205-215, 2009.

[22] Y. Itano, N. Itoh, S. Yoshitomi, and H. Hoshino, "High-Q MOS-varactor modeling for mm-wave VCOs," in *Microwave Conference Proceedings (APMC), 2012 Asia-Pacific*, 2012, pp. 202-204.

[23] S. Kitagawa, S. Suzuki, and M. Asada, "650-GHz Resonant-Tunneling-Diode VCO With Wide Tuning Range Using Varactor Diode," 2014.

[24] A. P. Hu, *Wireless/Contactless Power Supply:-Inductively coupled resonant converter solutions*: VDM Publishing, 2009.